PROCEEDINGS OF SCIENCE

The muon component of extensive air showers above $10^{17.5}$ eV measured with the Pierre Auger Observatory

Federico Sánchez[*a] **for the Pierre Auger Collaboration**[b†]

[a] *Instituto de Tecnologías en Detección y Astropartículas, CNEA-CONICET-UNSAM, Buenos Aires, Argentina*

[b] *Observatorio Pierre Auger, Av. San Martín Norte 304, 5613 Malargüe, Argentina*

E-mail: auger_spokespersons@fnal.gov

Full author list: http://www.auger.org/archive/authors_icrc_2019.html

The muon densities at 450 m from the core for showers above $10^{17.5}$ eV and zenith angle between 0° and 45° are presented. Results are based on 1 year of calibrated data collected by the engineering array of the Auger Muons and Infill for Ground Array (AMIGA) detector. Taking into account systematic uncertainties as well as attenuation effects, the observations suggest that the current hadronic interaction models fail in reproducing the measured number of muons with energies >1 GeV. Simulations at $10^{17.5}$ eV and $10^{18.0}$ eV show that for EPOS-LHC an increase of 38% is required at both energies, while for QGSJetII-04 an increment of 50% and 53% is needed at respective energies. Data have been combined with previous results on muon densities at higher energies showing the match in the evolution of the composition derived with the measurements of depth of the maximum development of the showers in the atmosphere ($X_{\rm max}$). The current AMIGA observations show that the variation of the primary masses has no sudden changes in the energy range $10^{17.5}$ to $10^{18.0}$ eV.

36th International Cosmic Ray Conference — ICRC2019
July 24th – August 1st, 2019
Madison, WI, U.S.A.

*Speaker.

†for collaboration list see PoS(ICRC2019)1177

PoS(ICRC2019)411

1. The AMIGA engineering array

The surface detector (SD) of the Pierre Auger Observatory [1] consists of an array of water-Cherenkov detector (WCD) placed in a triangular grid with spacing of 1500 m covering an area of 3000 km^2 (SD-1500), a smaller embedded array of 23.5 km^2 with 750 m spacing (SD-750), and finally an even denser array with 433 m spacing (SD-433) over 1.9 km^2. The fluorescence detector (FD) consists of 27 air-fluorescence telescopes overlooking the SD area from four sites. The contribution of Auger Muons and Infill for the Ground Array (AMIGA), alongside with the SD-750 and SD-433 arrays, is to provide a dedicated device to directly measure the muonic component of extensive air showers, the underground muon detector (UMD). Before proceeding to the construction of the full-size UMD, an array of prototypes operated until November 2017 to validate and optimize the detector design, and to evaluate its performances. This array, deployed at a depth of 2.3 m ($\sim$540 g/cm^2) to shield the electromagnetic component, was made with seven stations consisting in 30 m^2 of plastic scintillator. A detailed description of the present status of the underground muon detector array may be found in [2]. Once completed in the full SD-750 area, the UMD will serve as part of AugerPrime, the upgrade of the Observatory currently being deployed with the aim of improving the mass composition determination [3]. In this work, the first results based on the direct measurement of the muon densities of EAS in an energy region between 3×10^{17} eV and 2×10^{18} eV are presented. The analyzed data were collected during one year by the engineering array of AMIGA. In total, 1742 events with zenith angle up to 45° were analyzed. The full-sized UMD array will inlude 61 stations in the whole SD-750 area and is foreseen to be completed between the end of 2019 and mid 2020.

2. Detector efficiency and resolution

To determine the detector efficiency and to assess the resolution of the procedure for counting particles, one position of the array was equipped with identical *twin* underground scintillators triggered by the same water-Cherenkov detector. One unit was deployed towards the South of the surface detector, the other towards the North. For the resolution studies, we exploit the fact that two identical close-by detectors basically measure the same spot of the shower. Therefore, by analyzing the difference of their signals for a given event, it is possible to estimate signal fluctuations. As the separation between the twin detectors is $\sim$20 m, only signals at least 200 m away from the shower core are considered to be sampling the same muon density.

On the other hand, for efficiency analysis the different areas of the devices constituting the twin detector are used. In fact, the units of 30 m^2 are segmented into 2×10 m^2 and 2×5 m^2. The expected ratio of counts of two detectors of different areas is $r = \epsilon_1/\epsilon_2 \cdot a_1/a_2$ where ϵ_i is the efficiency of the detector with area a_i. An ideal counter of area a will record twice as many particles as a counter with an area $a/2$, and the ratio of counts between detectors will be $r = 2$. In the real case, a deviation from this behavior might arise, in particular if there are detection inefficiencies associated with the dimensions of the detectors. The joint probability to measure n_i and m_i particles for a single event i over two independent Poissonian detectors can be explicitly written in terms of the ratio of the expectation numbers $r = \mu_i/\nu_i$. The estimator for the ratio $\hat{r}$ is found by maximizing the corresponding likelihood function for N events leading to an estimator of the relative efficiency

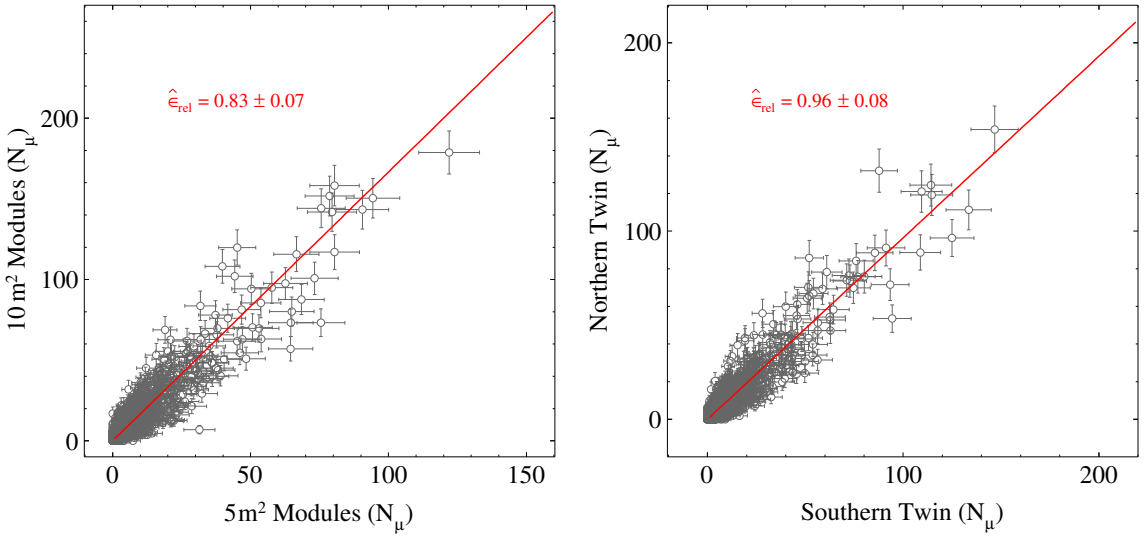

Figure 1: Relative efficiency between detectors of different (left) and identical (right) areas. The estimation $\hat{\epsilon}_{\rm rel}$ is obtained by fitting the data (red solid line).

between units of different area that can be written as $\hat{\epsilon}_{\rm rel} = {}^{a_2}/_{a_1} \cdot {}^{\bar{n}}/_{\bar{m}}$. The fraction ${}^{\bar{n}}/_{\bar{m}}$ is the ratio of the sample averages measured by the detectors with areas a_1 and a_2.

The twin position has eight modules, four of each area. By comparing the measurements on the four modules of $10\,{\rm m}^2$ with those of the four with $5\,{\rm m}^2$ area composing the *twin*, the relative efficiency between detectors can be assessed. The result of this comparison is shown in Fig. 1-(left). The relative signal efficiency estimation yields $\hat{\epsilon}_{\rm rel} = 0.83 \pm 0.07$. Within uncertainties, the obtained $\hat{\epsilon}_{\rm rel}$ is compatible with laboratory measurements [5]. This result is mainly driven by the attenuation of light along the fibers in the modules with larger area. Nevertheless, as soon as equal areas are compared, the twin devices behave as identical detectors. As an example, the case for $30\,{\rm m}^2$ is shown in Fig. 1-(right). This latter result is of major importance since it implies that the data from the twin detectors can be used to determine the resolution of the counting procedure.

Exploiting the same method used in the past to obtain the accuracy in the signal measurements of the SD stations [4], the sample variance σ^2 and mean N_μ estimators are calculated from the number N_i of muons measured by each twin on an event-by-event basis. Subsequently, the estimator

$$\Delta^2 \equiv \left(\frac{\sigma}{N_\mu}\right)^2 = 2\left(\frac{N_1 - N_2}{N_1 + N_2}\right)^2 \tag{2.1}$$

is evaluated for each event. The mean value of Δ^2 within bins of average number of muons is shown in Fig. 2-(left) as a function of the muon count. For an ideal counter, the resolution should be $\Delta^2_{\rm Poisson} = 1/N_\mu$. The blue line is the fit of a Poissonian model to the data. The counting uncertainty as a function of the number of counted muons results in

$$\Delta^2\left(N_\mu\right) = \frac{1.7 \pm 0.9}{N_\mu^{(1.0\pm0.2)}}. \tag{2.2}$$

As an illustration of the behavior of the UMD counters, the bin contents centered at 5 muons in Fig. 2-(right) are separately displayed and fitted with a Poissonian distribution. It is important to

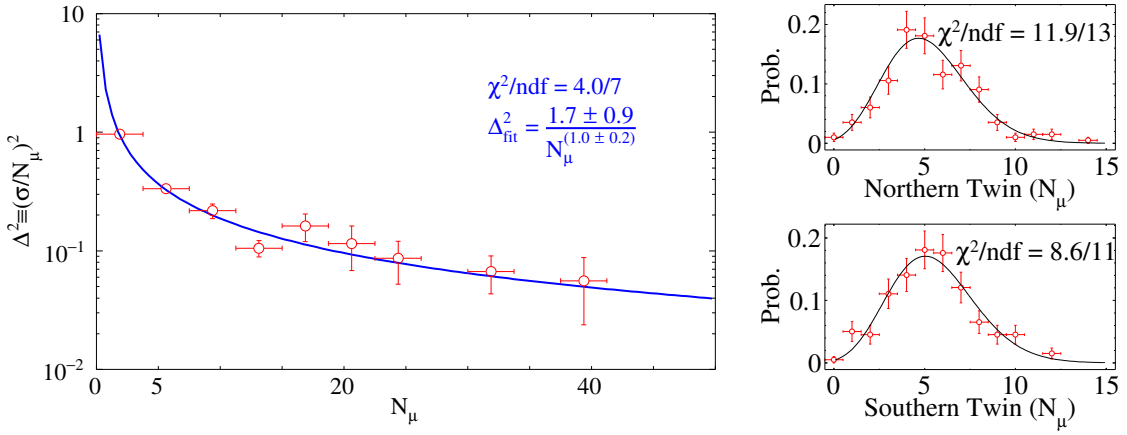

Figure 2: Resolution of the UMD. *Left:* Δ^2 as function of of average measured muons. The blue line is the fit of a Poissonian model. *Right:* From the bin $N_\mu = 5$, the distribution in each twin is shown alongside with its Poisson fit.

Source of Uncertainty	**Relative Systematic**
Calibration	3.9%
Soil density	2.8%
MLDF	8.8%
Efficiency correction	9.9%
CIC correction	2.3%
Total	**14.3%**

Table 1: Summary of analyzed systematic uncertainties (see text).

note that an ideal behavior of the counters is assumed for the construction of the likelihood model implemented in the muon lateral distribution function. Such an assumption is clearly supported by the data.

3. Systematic uncertainties

Five sources of systematic uncertainties have been studied in the present work [5]. These are: (i) the calibration procedure, (ii) the density variations of the soil covering the area of the detector, (iii) the unknown shape of the muon lateral distribution function, (iv) the area-dependent efficiency correction, and finally (v) the *Constant Intensity Cut* (CIC) correction to take into account the attenuation of muons in inclined showers. The impact of each source of uncertainty over the reconstructed muon density at the optimal distance of 450 m, ρ_{450}, is summarized in Tab. 1.

In the engineering UMD array, the counting of particles relied only on the signal amplitude, not on its charge. During this testing and developing phase, the selected optical sensors were multi-anode photo-multiplier tubes (MPMTs). The aim of the calibration was, therefore, to set the threshold of discrimination (V_{thr}) of each MPMT channel at the level of 30% of the single photo-

electron amplitude ($V_{\rm SPE}$). In total, 2240 channels were calibrated individually and the spread of thresholds after calibration routine was $\sigma = 21$ mV. Therefore, the detector response has been simulated for different values of $V_{\rm thr}$ ranging from 20% to 40% of $V_{\rm SPE}$ to estimate the effect of a 3σ variation. A relative uncertainty of $\sigma/\rho_{450} = 3.9\%$ is obtained from the linear fit.

The shielding of the electromagnetic component of EAS, as well as the energy of the muons that can reach the underground detectors, depends on the density of the soil. In-situ measurements of the density in three positions (two in the periphery and one in the center) of the SD-750 array were performed at depths of 1 m, 2 m, and 3 m. The mean measured soil density was 2.380 g/cm^3 with a dispersion of $\sigma = 0.051$ g/cm^3 between surveyed sites. Averaged over all considered angles, a relative systematic of $\sigma/\rho_{450} = 2.8\%$ is found.

When an extensive air shower falls within the detector array, each triggered station samples the density of muons ρ_μ at discrete distances from the shower core. The reconstruction procedure implies a fit with a pre-selected muon lateral distribution function (MLDF). For the underground muon detector, the chosen parametrization followed the KASCADE-Grande experiment [6],

$$\rho_\mu(r,E,\theta;\mathbf{p}) = \frac{A_\mu(E)}{A_0}\left(\frac{r}{r^*}\right)^{-\alpha}\left(1+\frac{r}{r^*}\right)^{-\beta(\theta;\mathbf{q})}\left(1+\left(\frac{r}{10r^*}\right)^2\right)^{-\gamma} \tag{3.1}$$

where $\mathbf{p} = \{r^*,\alpha,\gamma,\mathbf{q}\}$ are fixed parameters which were optimized with simulations and A_0 is a normalization factor. Only $A_\mu(E)$ is a free parameter. The simulation-based parametrization of the slope $\beta(\theta)$ adds additional systematic uncertainty. A conservative estimation of the corresponding uncertainty was performed by varying the slopes in $\pm 0.15\,\beta(\theta)$. Averaging over all angles $\theta \leq 48^\circ$, a mean relative systematic of $\sigma/\rho_{450} = 8.8\%$ is obtained.

During the reconstruction procedure the measured muon densities are corrected by area-dependent efficiency ϵ according to $\rho_\mu^{\rm corr} = \rho_\mu/\epsilon$. But the values of ϵ also depend on the time window in the signal used to identify muons [5]. To evaluate the associated systematic, the variation in ρ_{450} was calculated considering two cases: (i) when efficiencies associated to a time window of 22 ns are used, and (ii) when no inhibition window is set during the recontruction procedure. Averaged over the energy range from $10^{17.4}$ to $10^{18.3}$ eV, an uncertainty of $\sigma/\rho_{450} = 9.9\%$ is found.

As a result of the longer path in the atmosphere and the increased amount of soil covering the buried detectors, the muonic component of inclined air showers gets attenuated. Using UMD data, the attenuation function $f_{\rm att}(\theta;\mathbf{a},\mathbf{b})$ using the CIC method [7] was found. The muon density corrected by attenuation is therefore $\rho_{35} = \rho_{450}/f_{\rm att}(\theta)$. The uncertainties in the parameters $\{\mathbf{a},\mathbf{b}\}$ add additional systematic uncertainty. Averaged over the zenith-angle range $0^\circ \leq \theta \leq 45^\circ$ the mean relative uncertainty is 2.3%.

4. Results: ρ_{35} vs. Energy

For the analysis of data, the SD quality cuts were applied as for previous official reconstruction [8]. On top of that, as the UMD engineering array has seven stations, to ensure a good sampling of the shower by the underground detectors, the largest SD signal is required to be within the hexagon that constitutes the array of buried scintillators. The zenith-angle range was restricted to $\theta \leq 45^\circ$ to avoid large attenuation effects and statistical uncertainties due to the reduced areas of the scintillator plane. The energy as well as the geometry of the events are reconstructed using data

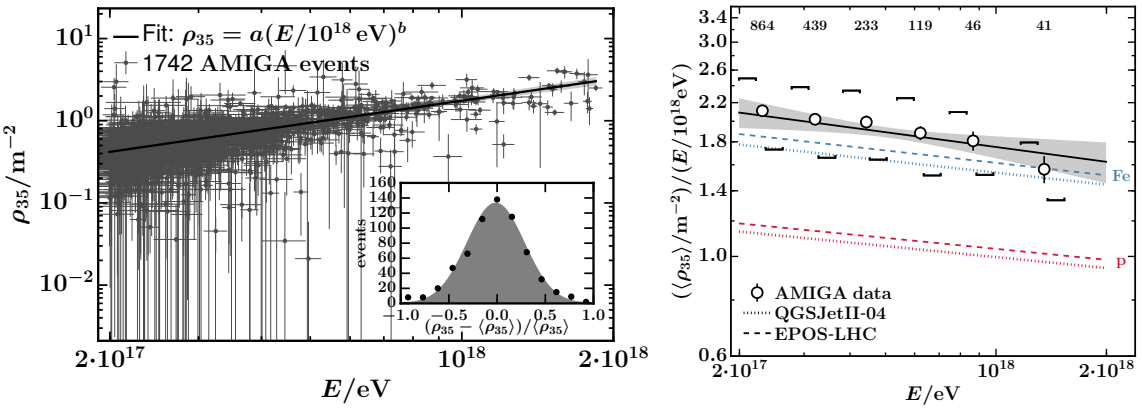

Figure 3: *Left:* Fit of the energy dependence $\rho_{35}(E;a,b)$ for AMIGA data. Vertical and horizontal error bars for single events correspond to the statistical errors. The inset shows the normalized residuals. *Right:* Energy-normalized densities as a function of E compared to expectations. Error bars denote the statistical uncertainties. Systematic uncertainties are indicated by square brackets. The number of events per bin is stated at the top. The obtained fit is shown by a black solid line with a shaded band corresponding to the statistical uncertainties.

from the SD-750 array alone. The reconstructed muon densities ρ_{35} as a function of the energy are shown in Fig. 3-(left). The evolution of ρ_{35} is fitted with a power law

$$\rho_{35}(E;a,b) = a\,(E/10^{18}\,\mathrm{eV})^b \tag{4.1}$$

by maximizing the log-likelihood function

$$\ln\mathscr{L} = \sum_k \ln\left(\sum_i e^{-\frac{(E_k-E_i)^2}{2\sigma_{E_i}^2}}\, e^{-\frac{(\rho_{35_k}-\rho_{35}(E_i;a,b))^2}{2\sigma_{\rho_{35_i}}^2}}\right). \tag{4.2}$$

The function of Eq. (4.2) accounts for the threshold effect that is caused by the application of an energy cut and accommodates the uncertainties both in the signal and energy estimate [9]. The energy uncertainty is σ_E (determined by the SD) while the uncertainty of the reconstructed muon densities is $\sigma_{\rho_{35}}$. The index k runs over events with energies above $10^{17.5}$ eV where the SD-750 array becomes fully efficient. The second sum with index i accounts for the migration of events below the full efficiency into the accepted energy range, by including events with energies above $10^{17.3}$ eV. The maximum considered energy is $10^{18.3}$ eV. The best fit solution is displayed by a solid line in Fig. 3-(left). The obtained values are $a = (1.75 \pm 0.05(\mathrm{stat}) \pm 0.05(\mathrm{sys}))/\mathrm{m}^2$ and $b = 0.89 \pm 0.04(\mathrm{stat}) \pm 0.04(\mathrm{sys})$ for the average muon density a at 10^{18} eV and the logarithmic gain b. The evolution of the muon content in data is compared to simulations with proton and iron primaries in Fig. 3-(right). To soften the strong energy dependence, the muon densities have been normalized by the energy. The slopes obtained from both hadronic interaction models are 0.91 for iron and 0.92 for proton, slightly steeper than found in the data. More strikingly, simulations fail to reproduce the observed muon densities which are between 8% (EPOS-LHC) and 14% (QGSJetII-04) larger than those obtained for iron showers at an energy of 10^{18} eV. In order to

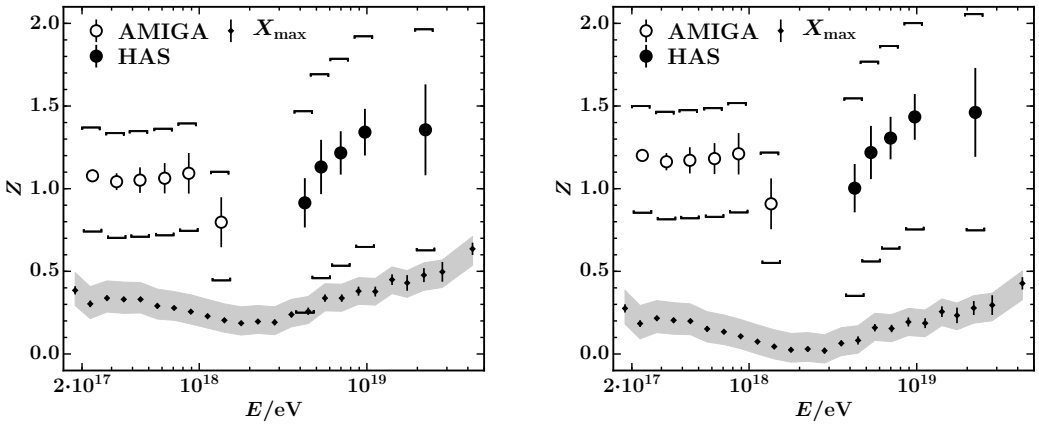

(a) EPOS-LHC (b) QGSJetII-04

Figure 4: z-factor from direct measurements of muons by AMIGA and the analysis of horizontal air showers (HASs) compared to the value coming from $\langle X_{\rm max}\rangle$ by the FD.

compare the muon densities measured by the AMIGA prototype array with the results of the study of the average number of muons in horizontal air shower (HAS) [10, 11], the z-factor [12]

$$z = \frac{\langle \ln \rho_{35}\rangle - \langle \ln \rho_{35}\rangle_{\rm p}}{\langle \ln \rho_{35}\rangle_{\rm Fe} - \langle \ln \rho_{35}\rangle_{\rm p}} \tag{4.3}$$

is calculated using simulations for proton and iron primary particles for a fixed energy and a specific hadronic interaction model. Replacing ρ_{35} by R_μ in Eq. (4.3), the z-factor is similarly obtained for the analysis of HAS. The results of both muon analyses are shown in Fig. 4 together with the corresponding values of $z = {}^{\ln A}/_{\ln 56}$ that are obtained from measurements of the depth of shower maximum $X_{\rm max}$ [13]. Within the statistical and systematic uncertainties, the z-factors derived by the two muon studies seem to be in agreement at the intermediate energies between their distinct energy ranges. Moreover, the combined muon measurements match the trend of z derived from $X_{\rm max}$ measurements as a function of the energy. To quantify the disagreement of the muon content between simulations and data, the combination of AMIGA muon densities with independent measurements of the mean depth of shower maximum of the fluorescence detector at fixed energies of $10^{17.5}$ and 10^{18} eV is presented. Using their linear dependence on the mean logarithmic mass, the mean logarithmic muon densities $\langle \ln \rho_{35}\rangle$ in simulations are related to the mean depth of shower maximum $\langle X_{\rm max}\rangle$ based on proton and iron simulations for both hadronic interaction models and primary energies. Comparing the muon densities measured by AMIGA with those in simulations in Fig. 5, we find that the muon content in simulations would need to be increased by 38% at both energies for EPOS-LHC while an increment of 50% at $10^{17.5}$ eV and 53% at 10^{18} eV is required for the QGSJetII-04 model to match the data.

5. Conclusions

Direct measurements of the muonic component of EAS with the Pierre Auger Observatory were presented for the first time. The observed muon densities, which are larger than for those from

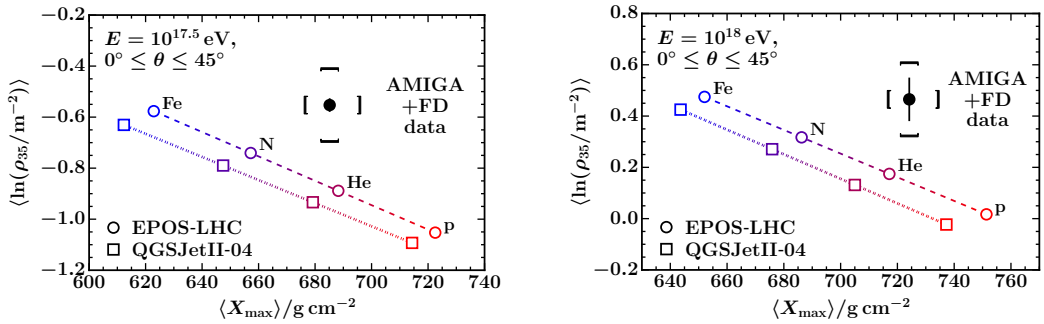

(a) $E = 10^{17.5}$ eV (b) $E = 10^{18}$ eV

Figure 5: Mean logarithmic muon density $\langle \ln \rho_{35} \rangle$ as a function of the mean depth of shower maximum $\langle X_{\max} \rangle$ for simulations with primary energies of $10^{17.5}$ eV (a) and 10^{18} eV (b) compared to Auger measurements with the FD ($\langle X_{\max} \rangle$) and AMIGA ($\langle \ln \rho_{35} \rangle$).

simulations, show the failure of current hadronic interaction models to reproduce the measurements in the considered energy range. The AMIGA prototype array results are in accordance to the previous Auger muon measurements of horizontal air showers at higher energies. Furthermore, the energy evolution of the combined muon measurements matches the expectations from the $X_{\max}$ measurements. The disagreement of the muon content measured by AMIGA and simulations has been quantified with the independent FD measurements of the mean depth of shower maxima. Similar evidence for a muon deficit in simulations were obtained by previous experiments, although direct comparisons are hindered by the different energy thresholds of the observed muons.

References

[1] The Pierre Auger Collaboration, Nucl. Instrum. Meth. A **798** (2015) 172–213

[2] A.M. Botti for the Pierre Auger Observatory, PoS(ICRC2019)202.

[3] A. Castellina for the Pierre Auger Observatory, EPJ Web Conf 210 (2019) 06002.

[4] M. Ave *et al.*, Nucl. Instrum. Meth. A **578** (2007) 180–184.

[5] S. Muller for the Pierre Auger Observatory, EPJ Web Conf 210 (2019) 02013.

[6] W.D. Apel *et al.*, Nucl. Instrum. Meth. A **620** (2010) 202–216.

[7] J. Hersil et al., Phys. Rev. Lett. **6** (1961) 22–23.

[8] F. Fenu for the Pierre Auger Collaboration, PoS(ICRC2017)486.

[9] H. Dembinski for the Pierre Auger Collaboration, Proc. 32$^{\text{th}}$ ICRC, (2011).

[10] L. Cazón for the Pierre Auger Collaboration, EPJ Web Conf 210 (2019) 02002.

[11] The Pierre Auger Collaboration, Phys. Rev. D **91** (2015) 032003.

[12] H. Dembinski for the Working Group on Hadronic Interactions and Shower Physics, EPJ Web Conf 210 (2019) 02004.

[13] J. Bellido for the Pierre Auger Collaboration, PoS(ICRC2017)506.